A REVIEW ON PHASE-VELOCITY AND FULL-WAVEFORM INVERSIONS OF SHALLOW-SEISMIC SURFACE WAVES

Y. Pan, L. Gao, and T. Bohlen

email: *Yudi.Pan@kit.edu*

keywords: *Surface waves, Dispersion, Full waveform, Inversion, Seismics*

ABSTRACT

Surface waves are widely used in near-surface geophysics and provide a non-invasive way to determine near-surface structures. By extracting and inverting dispersion curves to obtain local 1D S-wave velocity profiles, multichannel analysis of surface waves (MASW) has been proven as an efficient way to analyze shallow-seismic surface waves. By directly inverting the observed waveforms, full-waveform inversion (FWI) provides another feasible way to use surface waves in reconstructing near-surface structures. This paper provides a state of the art on MASW and shallow-seismic FWI and a comparison of both methods. A two-parameter numerical test is performed to analyze the nonlinearity of MASW and FWI, including the classical, the multiscale, the envelope-based, and the amplitude-spectrum-based FWI approaches. It shows that classical FWI and MASW have the highest and the lowest nonlinearity as well as resolution among these methods, respectively, while the modified FWI approaches have an intermediate nonlinearity and resolution between classical FWI and MASW.

INTRODUCTION

The reconstruction of near-surface elastic-parameter models is of fundamental importance for near-surface geophysical and geotechnical studies. Surface waves dominate the shallow-seismic wavefield and are attractive for determining near-surface structures due to their relatively high signal-to-noise ratio in field recordings. With a rapid development in the theories of surface-wave methods, it has become increasingly popular over the last two decades to use surface waves as a non-invasive way to estimate near-surface structures.

The spectral analysis of surface waves (SASW; Nazarian et al., 1983) marks the beginning of the shallow-seismic surface-wave methods. With the proposing of multichannel analysis of surface waves (MASW; Park et al., 1999; Xia et al., 1999) the methods began to flourish because MASW greatly improved the efficiency of surface-wave surveys by using a multistation approach. Both SASW and MASW use the dispersion characteristics of surface waves to determine near-surface structures, and a comparison between their performances is presented in Lin et al. (2017). Two main steps in MASW are the measuring and the inversion of the surface-wave dispersion curves (upper part in Fig. 1), which will be introduced in detail hereafter. Thus, many efforts have been made to improve the accuracy of surface-wave dispersion images (e.g., Park et al., 1998) and to reduce the nonuniqueness of the inverse problem (e.g., Xia et al., 1999; Socco and Boiero, 2008). A comprehensive review of MASW can be found in Socco et al. (2010).

Based on phase-velocity inversion, MASW assumes a 1D approximation of subsurface structures and allows the reconstruction of S-wave velocity as a function of depth. Different approaches have been proposed to account for lateral heterogeneity, such as cross-correlation analysis of multichannel data (Hayashi and Suzuki, 2004), spatial filter (Bohlen et al., 2004), and laterally constrained inversion (Socco et al., 2009). These approaches reduce the 2D effect in MASW, and make MASW applicable to not only layered but also laterally smoothly varying models. Due to the 1D layered model and the plane wave assumptions involved in the forward calculation of surface-wave dispersion curves, however, dispersion-curve-based

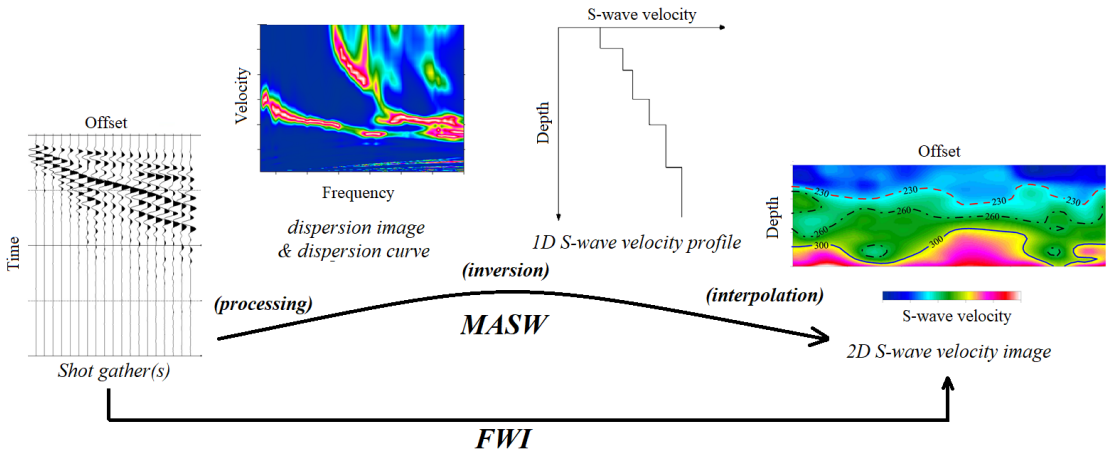

Figure 1: Comparison of MASW and FWI work flows.

methods fail to work when strong lateral heterogeneity exists, which is regarded as one of the limitations in MASW. Another problem that MASW faces is the difficulty in correctly estimating and identifying multi-modal dispersion curves (Zhang and Chan, 2003), especially when encountering low-velocity layers (Tsuji et al., 2012), strong vertical contrasts (De Nil, 2005), and a non-planar free surface (Zeng et al., 2012).

With a rapid increase in computational power it has become feasible to use full-waveform inversion (FWI; Tarantola, 1986) to resolve subsurface models by directly fitting the observed waveforms (lower part in Fig. 1). Based on full-wavefield modeling, FWI is able to fully exploit the waveform information and is getting increasingly popular on continental (Fichtner et al., 2008), explorational (Virieux and Operto, 2009), near-surface (Groos et al., 2017), and laboratory scales (Köhn et al., 2016). Due to the unique wavefield characteristics (e.g., frequency range and wave type) and the recording system in each scale, the application of FWI on different scales is not simply a matter of scale. For example, due to the existence of surface waves, the acoustic approximation, which is widely adopted in explorational seismic, is no longer valid in shallow seismic. The inclusion of surface waves in the wavefields also increases the nonlinearity of FWI (Gélis et al., 2007; Brossier et al., 2009). Bretaudeau et al. (2013) performed both numerical and laboratory experiments and demonstrated the potential of FWI in quantitatively imaging near-surface structures. Tran et al. (2013) applied a frequency-domain FWI to raw shallow-seismic Rayleigh-wave data to detect underground sinkholes. Masoni et al. (2013) compared the FWI objective functions in different data domains and showed that the use of multi-component surface-wave data can improve the well-posedness of FWI. Pérez Solano et al. (2014) proposed a windowed-amplitude waveform inversion method to invert shallow-seismic surface waves. Groos et al. (2014) studied the influence of attenuation in shallow-seismic FWI, and proposed to mitigate this influence by performing a source-wavelet correction. Nuber et al. (2015) presented a new scaling approach to enhance the sensitivities in the regions of interest (deep part of the model). Pan et al. (2016b) proposed a variable-grid time-domain Love-wave FWI algorithm and applied it to field data. Yuan et al. (2015), Wittkamp and Bohlen (2016) and Athanasopoulos and Bohlen (2016) proved the advantages of performing sequential and joint inversion of different shallow-seismic wave types. Dokter et al. (2017) and Tran and Sperry (2018) showed the high resolution of FWI for characterizing near-surface heterogeneity by using real-world examples. Nuber et al. (2017) studied the optimal geometry of field measurements for shallow-seismic FWI to improve the efficiency of shallow-seismic FWI. Borisov et al. (2017) presented a synthetic example of 3D FWI applied to surface and body waves in the presence of irregular surface topography using an envelope-based misfit function. Nuber et al. (2016) and Pan et al. (2018) studied the influence of free-surface topography on surface-wave FWI.

MASW uses the averaged phase velocity of multichannel data, which exploits the general part in the phase information of surface waves (i.e., averaged phase difference among multiple traces). Because the S-wave velocity derived from MASW is a kind of averaged layered result of the subsurface below the spread (Boiero and Socco, 2010), MASW suffers from relatively low resolution, especially when encountering

strong laterally heterogeneous models or heterogeneity of small scale. By using both phase and amplitude information, FWI has relatively higher resolution and better applicability to heterogeneous models. FWI is an ill-posed problem and could converge toward a local minimum (Virieux and Operto, 2009). An effective way to reduce the ambiguity of FWI is to use an appropriate initial model provided by MASW (Pan et al., 2017). Other approaches like multiscale FWI (MFWI; Bunks et al., 1995; Groos et al., 2017), envelope-based FWI (EFWI; Bozdağ et al., 2011; Wu et al., 2014), and amplitude-spectrum-based FWI (AFWI; Pérez Solano et al., 2014; Dou and Ajo-Franklin, 2014) could also mitigate the ill-posedness of FWI. However, there are no detailed comparisons between the performances of MASW and FWI; consequently, how to appropriately choose them to process shallow-seismic surface waves is unclear.

In this paper, we compare MASW and FWI in reconstructing near-surface structures. We first illustrate the main steps in MASW and FWI, including classical FWI and three modified FWI approaches (MFWI, EFWI, and AFWI). We draw some links among these methods by discussing the subdata they use and compare the ill-posedness of them by using a numerical example.

MULTICHANNEL ANALYSIS OF SURFACE WAVES (MASW)

In a layered model, surface-wave phase velocity V_{ph} is determined by an equation D in a nonlinear, implicit form as

$$D(V_{ph}(f), \mathbf{m}) = 0\,, \tag{1}$$

where f represents frequency, and $\mathbf{m}$ represents elastic model parameters (v_p, v_s, and ρ) as a function of depth (1D). We can calculate the surface-wave phase velocity by solving the forward equation D numerically via means like Thomson-Haskell method (Thomson, 1950), Knopoff method (Knopoff, 1964), reflection and transmission coefficients method (Chen, 1993), or delta-matrix method (Watson, 1970).

In MASW, we aim at minimizing the misfit between synthetic and observed dispersion curves (phase velocities over different frequencies), which can be written as

$$\Phi_{MASW}(\mathbf{m}) = \frac{1}{2}\sum_{s_r}\sum_{f}\|V_{ph}^{syn}(f) - V_{ph}^{obs}(f)\|^2 \tag{2}$$

where $V_{ph}^{syn}(f)$ and $V_{ph}^{obs}(f)$ are the synthetic and observed dispersion curves, respectively; s_r denotes the sources. The misfit function may also be weighted using a data covariance matrix (Xia et al., 2010), or it can be stabilized by adding model constraints (Piatti et al., 2013). However, we do not incorporate them here for the sake of brevity.

Two main steps involved in MASW are the measuring and the inversion of dispersion curves (Fig. 1). For the measuring of surface-wave dispersion curves, we need to transform the wavefield data from the space-time (x-t) domain to the frequency-wavenumber (f-k) or the frequency-velocity (f-v) domain. Then we pick the continuous dispersive-energy peaks over different frequencies as surface-wave dispersion curves. The measuring of surface-wave dispersion curves can be expressed as

$$U(f,k) = \sum_{l} S_l(f)\cdot\sum_{r_n} e^{i[k(f)-k_l(f)]\cdot r_n} \tag{3}$$

where $U(f,k)$ represents the surface-wave spectrum in the f-k domain, which is also called dispersion image. S_l represents a source function of the lth mode, r_n is the distance between the source and the nth receiver; k_l is the wavenumber (frequency divided by phase velocity) of the lth mode, $k(f)$ is the picked dispersion curve in the f-k domain, which is equivalent to $V_{ph}(f)$ in the f-v domain ($V_{ph}^{obs}(f)$ in equation 2). The spatial change in k_l, which could indicate the lateral variation of the model (Strobbia and Foti, 2006), however, is neglected in the multichannel data set. It should be noted that above expression is not valid in the near field due to the plane-wave (high-frequency) approximation (Aki and Richards, 2002). In layered or laterally smoothly varying models, the picked dispersion curve represents a harmonic mean of the velocity structure below the spread (Boiero and Socco, 2010).

We assume that a clear and continuous dispersive energy peak in the dispersion image represents an individual mode of surface waves. This assumption is valid in most cases. However, a visually continuous energy peak may shift from one mode to another at a certain frequency point. This phenomenon is called

mode osculation (Boaga et al., 2013) or mode kissing (Xia et al., 2012). Because it is almost impossible to identify the conversion between different modes in a continuous energy peak by using one dispersion image alone, it is recommended to use multi-component data (Ikeda et al., 2014) or to jointly use Rayleigh- and Love-wave data (Gao et al., 2016) to reduce the possibility in the misidentification of surface-wave dispersion curves.

Many algorithms have been proposed to invert surface-wave dispersion curves, including both local search methods based on a gradient or Jacobian matrix (Fréchet derivative) (e.g., Xia et al., 1999) and global search methods that solve the optimization problem stochastically (e.g., Yamanaka and Ishida, 1996; Socco and Boiero, 2008; Boaga et al., 2011; Song et al., 2012). By interpolating multiple 1D profiles estimated from different spreads using MASW, the lateral variation can then be partly retrieved in a pseudo 2D (Bohlen et al., 2004; Luo et al., 2009; Mi et al., 2017) or 3D model (Boiero et al., 2011; Strobbia et al., 2011; Ikeda and Tsuji, 2015; Pan et al., 2016a). Because we only use planar surface waves in MASW, the phase information related to some of the non-layered structures (e.g., scattered surface waves caused by lateral heterogeneity; Chai et al., 2012; Bergamo and Socco, 2014; Sloan et al., 2015) is excluded after picking the dispersion curve since these waves do not behave as a dispersive continuous energy trend in the f-v domain. This is another reason for the difficulty to nicely reconstruct those non-layered structures using MASW.

FULL-WAVEFORM INVERSION (FWI)

Classical FWI

The relationship between the seismic wavefield u and an elastic model $\mathbf{m}$ (1D, 2D, or 3D) can be written as

$$u(t) = G(\mathbf{m}) * S(t) \tag{4}$$

where $G(\mathbf{m})$ denotes the Green's function of a model $\mathbf{m}$, $S(t)$ denotes a seismic source time function (STF), and the symbol $*$ represents convolution in the time domain. Equation 4 can be simulated by solving the wave equation numerically. In this paper, we adopt a staggered-grid finite-difference method (FDM) as a forward solver to simulate 2D elastic (P-SV) waves (Virieux, 1986).

FWI aims at minimizing the misfit between synthetic and observed waveforms. In classical FWI (CFWI), the L2-norm misfit function Φ_{CFWI} is defined as

$$\Phi_{CFWI}(\mathbf{m}) = \frac{1}{2} \sum_{s_r, x_r} \int_0^T \|u^{syn}(t, x_r) - u^{obs}(t, x_r)\|^2 dt \tag{5}$$

where u^{syn} and u^{obs} denotes the synthetic and observed waveforms, respectively. s_r and x_r represents the sources and receivers, respectively, and T represents the total recording time. Though we could use different norms to define the objective function (Brossier et al., 2010), here we use the L2-norm so that both MASW and FWI objective functions are based on the same least-squares definition.

Although attempts have been made in using global optimization algorithms to solve the inverse problem in FWI, most of the FWI studies use gradient-based local optimization algorithms due to a tremendous number of parameters in $\mathbf{m}$. The huge number of parameters also makes the direct numerical calculation of the Jacobian matrix (Fréchet derivative) computational expensive. The gradient of the FWI misfit function with respect to model parameters, however, can be efficiently calculated using an adjoint state algorithm (Plessix, 2006), in which only two wavefield simulations are needed: One simulation of the forward-propagating wavefield (state variable), and one simulation of the back-propagating residual wavefield (adjoint-state variable). The gradient can be calculated by correlating the state and the adjoint-state variables. By iteratively updating the model $\mathbf{m}$ with a local optimization algorithm either incorporating the Hessian matrix (e.g., Quasi-Newton algorithm, Gauss-Newton algorithm, truncated Newton algorithm) or not (e.g., steepest-descent algorithm, conjugate gradient algorithm), we can finally obtain a physical model which can explain the observed waveforms appropriately.

Modified FWI approaches

The classical FWI misfit function is affected by the existence of numerous local minima, which greatly increases the ill-posedness of the inverse problem. One efficient way to reduce the possibility of getting trapped in a local minimum is to adopt an appropriate initial model that is close to the true model. However, the building of an appropriate initial model cannot always be guaranteed in real-world cases. Another way to mitigate the nonlinearity of FWI is to modify its objective function. Three approaches that have been proposed and applied to shallow-seismic data are the multiscale FWI (Bunks et al., 1995; Groos et al., 2017), the amplitude-spectra-based FWI (Pérez Solano et al., 2014), and the envelope-based FWI (Bozdağ et al., 2011; Wu et al., 2014; Yuan et al., 2015).

In MFWI we start at inverting the low-frequency part (long-wavelength) of the data, and then progressively introduce high-frequency (short-wavelength) content in the data space. It can be expressed as

$$\Phi_{MFWI}(\mathbf{m}) = \frac{1}{2}\sum_{s_r,x_r}\int_0^T \|F[u^{syn}(t,x_r)] - F[u^{obs}(t,x_r)]\|^2\,dt \tag{6}$$

where F represents a frequency filter. MFWI provides a natural framework to perform the scale separation of the data by using different frequency filters. It uses a subset of the data which only contains the long-wavelength (low-frequency) components to reconstruct a general background model in the beginning stage, and then progressively includes the data of shorter wavelengths (higher frequencies) to reconstruct structures of smaller scales. MFWI becomes equivalent to CFWI when the frequency filter covers the whole range of interest.

In AFWI a new misfit function Φ_{AFWI} is designed as

$$\Phi_{AFWI}(\mathbf{m}) = \frac{1}{2}\sum_{s_r,w}\int_0^{f_{max}}\int_0^{k_{max}} \|\,|U_w^{syn}(f,k)| - |U_w^{obs}(f,k)|\,\|^2\,df\,dk \tag{7}$$

where $U_w^{syn}(f,k)$ and $U_w^{obs}(f,k)$ represent the f-k spectra of the spatially windowed synthetic and observed data, respectively. The parameter w represents the spatial windows, and $|.|$ represents the absolute value of a complex number. The data space of AFWI has been transformed from the *x*-*t* domain to the f-k domain, and AFWI tries to minimize the difference between the amplitude spectra of the observed and synthetic waveforms.

By defining the misfit associated with surface-wave dispersion spectra (U in equations 3 and 7), AFWI can be viewed as an intermediate way between MASW and the classical FWI. AFWI avoids the ambiguity caused by the picking of modal dispersion curves in MASW and also includes amplitude information of surface waves in the inversion. AFWI is similar to a modified MASW method presented in Forbriger (2003) and Ryden and Park (2006), in which the inversion tries to minimize the difference between an observed phase-velocity spectrum and that simulated from a theoretical layered model. AFWI adopts a 2D forward solver while the modified MASW method is based on a 1D structure; thus, AFWI is more applicable to laterally heterogeneous models than the modified MASW method.

In AFWI cycle skipping happens when the inversion tries to fit a single-mode surface-wave spectrum by another mode, and is equivalent to a mode misidentification of surface waves in MASW (Zhang and Chan, 2003). This means, the wider the surface-wave energy trend (equivalently, the lower the resolution in the wavenumber domain), the less possible it is that AFWI will be trapped in a local minimum. Since the resolution of a surface-wave energy trend in the wavenumber domain is inversely proportional to the length of the spread (Forbriger, 2003), AFWI is able to balance the resolution of the f-k spectra to avoid cycle skipping by incorporating spatial windows of different lengths (Pérez Solano et al., 2014).

In EFWI, the misfit function Φ_{EFWI} is defined as

$$\Phi_{EFWI}(\mathbf{m}) = \frac{1}{2}\sum_{s_r,x_r}\int_0^T \|[e^{syn}(t,x_r)]^p - [e^{obs}(t,x_r)]^p\|^2\,dt \tag{8}$$

where e^{syn} and e^{obs} are the envelopes of synthetic and observed waveforms, respectively. The parameter p is the power for the envelope data and is usually chosen as 1 in shallow seismic (Yuan et al., 2015). The

envelope function e can be obtained via Hilbert transform as

$$e(t, x_r) = \sqrt{u^2(t, x_r) + H^2[u(t, x_r)]} \tag{9}$$

with H denoting the Hilbert transform.

Similar to MFWI, EFWI also uses the long-wavelength part of the data in its first stage. However, it performs a nonlinear scale separation by an envelope operator and, thus, has the ability to extract ultra-low-frequency signals (Wu et al., 2014).

Overall, MFWI, AFWI, and EFWI are different hierarchical strategies in FWI. All of them firstly invert a part of the data (subdata) that is less sensitive to cycle skipping. By choosing appropriate frequency filters (F in equation 6), spatial windows (w in equation 7), and numbers of power (p in equation 8), MFWI, AFWI, and EFWI are able to separate the data into different scales, so that each modified FWI approach provides a multi-stage hierarchical FWI strategy. These three approaches share the same adjoint-state equation with CFWI. In other words, the only difference in their gradient calculations exists in their adjoint sources, which is related to their corresponding objective function. By incorporating spatial windows, however, AFWI has a higher computational cost compared to the others because the misfit gradient needs to be calculated for each window.

NUMERICAL EXAMPLE

A layered model (Table 1) is used to compare the performances of MASW and FWI (including both the classical and the three modified FWI approaches) in reconstructing near-surface structures. The observed and synthetic waveforms for FWI are simulated by FDM. A 25 Hz Ricker wavelet with 50 ms delay is used as STF, and is generated as a vertical force. Forty-eight two-component receivers are placed along the free surface with a nearest offset of 4 m and a trace interval of 1 m; they record both vertical and horizontal components. The observed and synthetic input data for MASW is the fundamental-mode dispersion curve from 10 to 80 Hz with an interval of 2 Hz, which is calculated via the Thomson-Haskell method (Haskell, 1953).

Table 1: A simple layered model for numerical testing.

	S-wave velocity (m/s)	P-wave velocity (m/s)	density (g/cm^3)	thickness (m)
Layer 1	200	500	2.0	5
Half space	400	1000	2.0	∞

Since surface waves are much more sensitive to the S-wave velocity compared to the P-wave velocity and density in both MASW and FWI (Xia et al., 1999; Groos et al., 2017), we only test the influence of the S-wave velocity (Vs) on the objective functions of MASW and FWI. The Vs model consists of two values: a top-layer velocity Vs_top, which ranges from 100 to 300 m/s, and a homogeneous half-space (bedrock) velocity Vs_bedrock that ranges from 300 to 500 m/s. We use the true P-wave velocity and density models (Table 1) in all synthetic tests.

We perform a series of two-parameter inversion test on each method, respectively, to compare their dependence on the initial model. The model space is that Vs_top ranges from 100 to 300 m/s, and Vs_bedrock ranges from 300 to 500 m/s. We adopt a conjugate-gradient (CG) algorithm (Hestenes and Stiefel, 1952) as the optimization algorithm. The gradient of the objective function is calculated by a finite-difference approximation (Nocedal and Wright, 2006).

The initial model is chosen in the whole model space with a grid spacing of 4 m/s. Fig. 2 shows the solution paths in MASW and EFWI when an initial model with Vs_top $=$ 104 m/s and Vs_bedrock $=$ 304 m/s is chosen (starting point in Fig. 2). Both MASW and EFWI successively find the global minimum, while MASW needs fewer iterations compared to EFWI. When using the same initial model in the other cases (CFWI, AFWI, MFWI), however, the solution path goes out of the model space, which is regarded as a divergence in the inverse problem.

After performing inversion tests on all initial models in the model space, 98% of the models can successfully converge to the global minimum in MASW (red asterisks in the top-left image in Fig. 3). Those

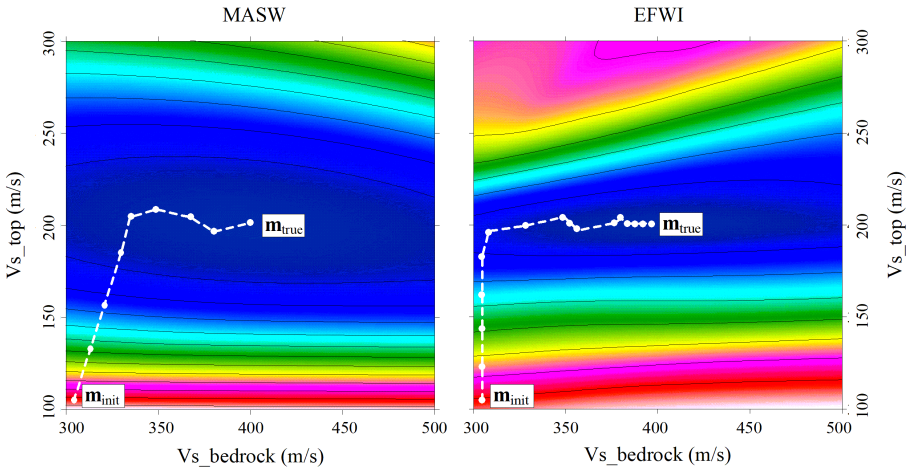

Figure 2: Examples of solution paths for MASW and EFWI in the two-parameter inversion examples. Dashed lines and dots are the solution paths and iterative solutions, respectively. The starting point (initial model) in these two examples is Vs_top = 104 m/s and Vs_bedrock = 304 m/s.

'divergent' points (starting models which fail to converge to the global minimum; blue asterisks in the top-left image in Fig. 3) are mainly located at the boundaries of the model space. Some of them are treated as 'divergent' because our model space is not big enough to search for their solution paths which may finally lead towards the global minimum. In other words, some of the 'divergent' points located at the boundaries of the model space may become 'convergent' if we expand our model space. Overall, this inversion test shows a relatively low dependence of MASW on the initial model.

Similarly, we can find the global minimum by using 17%, 72%, 65%, and 94% of the initial models in CFWI, MFWI, AFWI, and EFWI, respectively. In CFWI, most of the 'convergent' points are located in a region where Vs_top is less than 10% off its true value, and only 17% of the starting points in the model space are able to converge to the global minimum. It shows a high dependence of CFWI on the initial model. This dependence on the initial model is greatly reduced when a modified approach is adopted. In the cases of MFWI and AFWI, more 'convergent' points are located in a region where Vs_top is higher than its true value compared to the other side. This is because these methods primarily use the kinematic information (traveltime) of the data, which is reciprocal to the velocity value. Thus, a higher velocity has less influence on the kinematic information of the data. This behavior provides a useful suggestion when preparing an initial model for these methods. Overall, these inversion tests prove that the success of CFWI is highly dependent on the initial model, while this dependence decreases when incorporating the hierarchical approach (adopting a modified FWI approach). MASW has a lower dependence on the initial model, which can be used to provide an appropriate initial model for FWI.

CONCLUSIONS

Both multichannel analysis of surface wave (MASW) and full-waveform inversion (FWI) provide ways to use shallow-seismic surface waves in reconstructing near-surface structures. A numerical example was performed to compare the shapes of the objective functions of MASW, classical FWI, and three modified FWI approaches including multiscale FWI, envelope-based FWI, and spectrum-based FWI. The comparison showed that MASW possesses high stability but a relatively low resolution in imaging near-surface structures, while classical FWI behaves just the other way round, and the modified FWI approaches provide an intermediate stability and resolution between MASW and classical FWI. These characteristics were also proven by the synthetic inversion test. It led to the idea that a sequential strategy in which MASW, a (or some) modified FWI approach(es), and classical FWI are progressively used could provide a stable hierarchical way for the high-resolution imaging of near-surface structures.

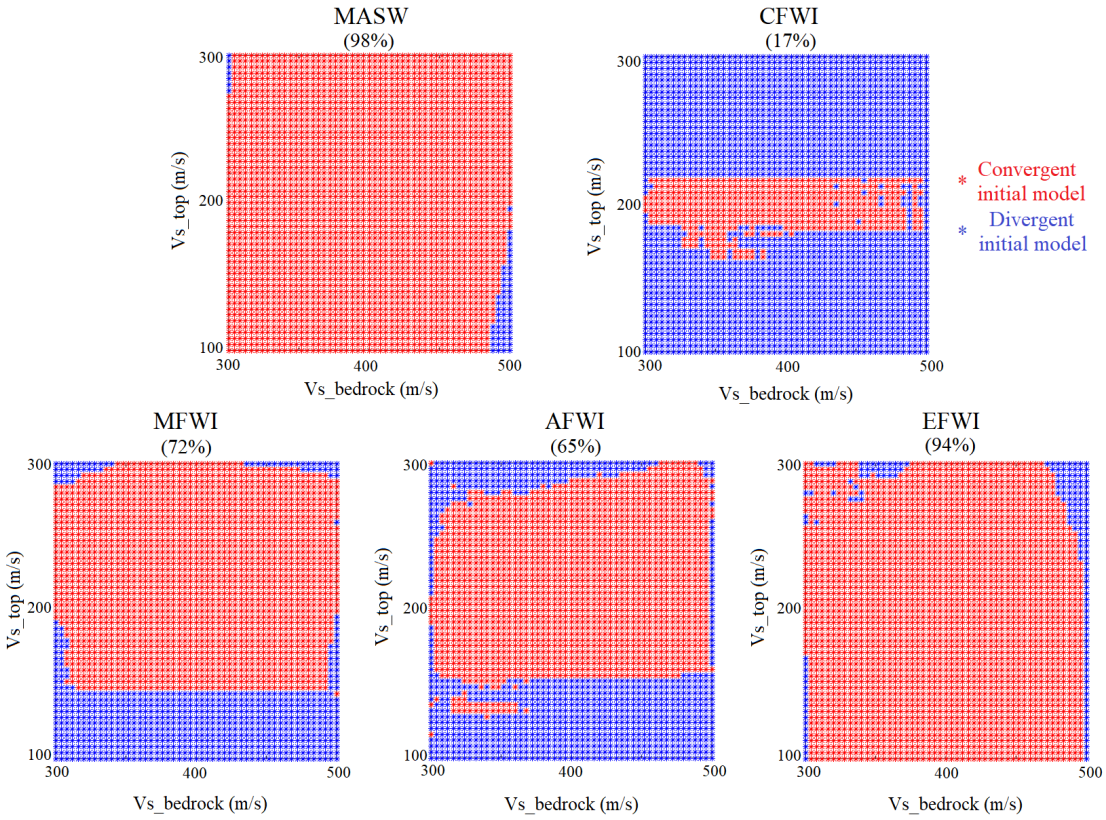

Figure 3: Distribution of convergent and divergent initial models of MASW, CFWI, MFWI, AFWI, and EFWI in the two-parameter inversion examples. Red and blue asterisks are the starting points (initial models) which converge toward or diverge from the global minimum, respectively.

ACKNOWLEDGMENTS

This work was kindly supported by the sponsors of the Wave Inversion Technology (WIT) consortium.

PUBLICATION

An extended version of this WIT article was submitted for publication in *Surveys in Geophysics*.

REFERENCES

Aki, K. and Richards, P. G. (2002). *Quantitative seismology*. University Science Books.

Athanasopoulos, N. and Bohlen, T. (2016). Sequential full-waveform inversion of refracted and Rayleigh waves. In *Near Surface Geoscience 2016, 22nd European Meeting of Environmental and Engineering Geophysics*.

Bergamo, P. and Socco, L. V. (2014). Detection of sharp lateral discontinuities through the analysis of surface-wave propagation. *Geophysics*, 79(4):EN77–EN90.

Boaga, J., Cassiani, G., Strobbia, C. L., and Vignoli, G. (2013). Mode misidentification in Rayleigh waves: Ellipticity as a cause and a cure. *Geophysics*, 78(4):EN17–EN28.

Boaga, J., Vignoli, G., and Cassiani, G. (2011). Shear wave profiles from surface wave inversion: the impact of uncertainty on seismic site response analysis. *Journal of Geophysics and Engineering*, 8(2):162.

Bohlen, T., Kugler, S., Klein, G., and Theilen, F. (2004). 1.5D inversion of lateral variation of Scholte wave dispersion. *Geophysics*, 69(2):330–344.

Boiero, D., Bergamo, P., Bruno Rege, R., and Socco, L. V. (2011). Estimating surface-wave dispersion curves from 3D seismic acquisition schemes: Part 1–1D models. *Geophysics*, 76(6):G85–G93.

Boiero, D. and Socco, L. V. (2010). Retrieving lateral variations from surface wave dispersion curves. *Geophysical Prospecting*, 58(6):977–996.

Borisov, D., Modrak, R., Gao, F., and Tromp, J. (2017). 3D elastic full-waveform inversion of surface waves in the presence of irregular topography using an envelope-based misfit function. *Geophysics*, 83(1):1–45.

Bozdağ, E., Trampert, J., and Tromp, J. (2011). Misfit functions for full waveform inversion based on instantaneous phase and envelope measurements. *Geophysical Journal International*, 185(2):845–870.

Bretaudeau, F., Brossier, R., Leparoux, D., Abraham, O., and Virieux, J. (2013). 2D elastic full-waveform imaging of the near-surface: Application to synthetic and physical modelling data sets. *Near Surface Geophysics*, 11(3):307–316.

Brossier, R., Operto, S., and Virieux, J. (2009). Seismic imaging of complex onshore structures by 2D elastic frequency-domain full-waveform inversion. *Geophysics*, 74(6):WCC105–WCC118.

Brossier, R., Operto, S., and Virieux, J. (2010). Which data residual norm for robust elastic frequency-domain full waveform inversion? *Geophysics*, 75(3):R37–R46.

Bunks, C., Saleck, F. M., Zaleski, S., and Chavent, G. (1995). Multiscale seismic waveform inversion. *Geophysics*, 60(5):1457–1473.

Chai, H.-Y., Phoon, K.-K., Goh, S.-H., and Wei, C.-F. (2012). Some theoretical and numerical observations on scattering of Rayleigh waves in media containing shallow rectangular cavities. *Journal of Applied Geophysics*, 83:107–119.

Chen, X. (1993). A systematic and efficient method of computing normal modes for multilayered half-space. *Geophysical Journal International*, 115(2):391–409.

De Nil, D. (2005). Characteristics of surface waves in media with significant vertical variations in elasto-dynamic properties. *Journal of Environmental and Engineering Geophysics*, 10(3):263–274.

Dokter, E., Köhn, D., Wilken, D., Nil, D., and Rabbel, W. (2017). Full-waveform inversion of SH- and Love-wave data in near-surface prospecting. *Geophysical Prospecting*, 65:216–236.

Dou, S. and Ajo-Franklin, J. B. (2014). Full-wavefield inversion of surface waves for mapping embedded low-velocity zones in permafrost. *Geophysics*, 79(6):EN107–EN124.

Fichtner, A., Kennett, B. L., Igel, H., and Bunge, H.-P. (2008). Theoretical background for continental- and global-scale full-waveform inversion in the time–frequency domain. *Geophysical Journal International*, 175(2):665–685.

Forbriger, T. (2003). Inversion of shallow-seismic wavefields: I. Wavefield transformation. *Geophysical Journal International*, 153(3):719–734.

Gao, L., Xia, J., Pan, Y., and Xu, Y. (2016). Reason and condition for mode kissing in MASW method. *Pure and Applied Geophysics*, 173(5):1627–1638.

Gélis, C., Virieux, J., and Grandjean, G. (2007). Two-dimensional elastic full waveform inversion using Born and Rytov formulations in the frequency domain. *Geophysical Journal International*, 168(2):605–633.

Groos, L., Schäfer, M., Forbriger, T., and Bohlen, T. (2014). The role of attenuation in 2D full-waveform inversion of shallow-seismic body and Rayleigh waves. *Geophysics*, 79(6):R247–R261.

Groos, L., Schäfer, M., Forbriger, T., and Bohlen, T. (2017). Application of a complete workflow for 2D elastic full-waveform inversion to recorded shallow-seismic Rayleigh waves. *Geophysics*, 82(2):R109–R117.

Haskell, N. A. (1953). The dispersion of surface waves on multilayered media. *Bulletin of the seismological Society of America*, 43(1):17–34.

Hayashi, K. and Suzuki, H. (2004). CMP cross-correlation analysis of multi-channel surface-wave data. *Exploration Geophysics*, 35(0):7–13.

Hestenes, M. R. and Stiefel, E. (1952). *Methods of conjugate gradients for solving linear systems*, volume 49. NBS.

Ikeda, T., Matsuoka, T., Tsuji, T., and Nakayama, T. (2014). Characteristics of the horizontal component of Rayleigh waves in multimode analysis of surface waves. *Geophysics*, 80(1):EN1–EN11.

Ikeda, T. and Tsuji, T. (2015). Advanced surface-wave analysis for 3D ocean bottom cable data to detect localized heterogeneity in shallow geological formation of a CO2 storage site. *International Journal of Greenhouse Gas Control*, 39:107–118.

Knopoff, L. (1964). A matrix method for elastic wave problems. *Bulletin of the Seismological Society of America*, 54(1):431–438.

Köhn, D., Meier, T., Fehr, M., Nil, D., and Auras, M. (2016). Application of 2D elastic Rayleigh waveform inversion to ultrasonic laboratory and field data. *Near Surface Geophysics*, 14(5):461–476.

Lin, C.-P., Lin, C.-H., and Chien, C.-J. (2017). Dispersion analysis of surface wave testing– SASW vs. MASW. *Journal of Applied Geophysics*, 143:223–230.

Luo, Y., Xia, J., Liu, J., Xu, Y., and Liu, Q. (2009). Research on the middle-of-receiver-spread assumption of the MASW method. *Soil Dynamics and Earthquake Engineering*, 29(1):71–79.

Masoni, I., Brossier, R., Virieux, J., and Boelle, J. (2013). Alternative misfit functions for fwi applied to surface waves. In *75th EAGE Conference & Exhibition incorporating SPE EUROPEC 2013*.

Mi, B., Xia, J., Shen, C., Wang, L., Hu, Y., and Cheng, F. (2017). Horizontal resolution of multichannel analysis of surface waves. *Geophysics*, 82(3):EN51–EN66.

Nazarian, S., Stokoe, I., Kenneth, H., and Hudson, W. (1983). *Use of spectral analysis of surface waves method for determination of moduli and thicknesses of pavement systems*. Number 930.

Nocedal, J. and Wright, S. (2006). *Numerical optimization*. Springer.

Nuber, A., Manukyan, E., and Maurer, H. (2015). Enhancement of near-surface elastic full waveform inversion results in regions of low sensitivities. *Journal of Applied Geophysics*, 122:192–201.

Nuber, A., Manukyan, E., and Maurer, H. (2016). Ground topography effects on near-surface elastic full waveform inversion. *Geophysical Journal International*, 207(1):67–71.

Nuber, A., Manukyan, E., and Maurer, H. (2017). Optimizing measurement geometry for seismic near-surface full waveform inversion. *Geophysical Journal International*, 210(3):1909–1921.

Pan, Y., Gao, L., and Bohlen, T. (2017). Sequential phase-velocity and waveform inversion of shallow-seismic surface waves–A field example for bedrock mapping. In *23rd European Meeting of Environmental and Engineering Geophysics*.

Pan, Y., Gao, L., and Bohlen, T. (2018). Time-domain full-waveform inversion of Rayleigh and Love waves in presence of free-surface topography. *Journal of Applied Geophysics*, 152:77–85.

Pan, Y., Xia, J., Xu, Y., and Gao, L. (2016a). Multichannel analysis of Love waves in a 3D seismic acquisition system. *Geophysics*, 81(5):EN67–EN74.

Pan, Y., Xia, J., Xu, Y., Gao, L., and Xu, Z. (2016b). Love-wave waveform inversion for shallow shear-wave velocity using a conjugate gradient algorithm. *Geophysics*, 81(1):R1–R14.

Park, C. B., Miller, R. D., and Xia, J. (1999). Multichannel analysis of surface waves. *Geophysics*, 64(3):800–808.

Park, C. B., Miller, R. D., Xia, J., et al. (1998). Imaging dispersion curves of surface waves on multi-channel record. In *1998 SEG Annual Meeting*. Society of Exploration Geophysicists.

Pérez Solano, C., Donno, D., and Chauris, H. (2014). Alternative waveform inversion for surface wave analysis in 2-D media. *Geophysical Journal International*, 198(3):1359–1372.

Piatti, C., Socco, L., Boiero, D., and Foti, S. (2013). Constrained 1D joint inversion of seismic surface waves and P-refraction traveltimes. *Geophysical Prospecting*, 61(s1):77–93.

Plessix, R. (2006). A review of the adjoint-state method for computing the gradient of a functional with geophysical applications. *Geophysical Journal International*, 167(2):495–503.

Ryden, N. and Park, C. B. (2006). Fast simulated annealing inversion of surface waves on pavement using phase-velocity spectra. *Geophysics*, 71(4):R49–R58.

Sloan, S. D., Peterie, S. L., Miller, R. D., Ivanov, J., Schwenk, J. T., and McKenna, J. R. (2015). Detecting clandestine tunnels using near-surface seismic techniques. *Geophysics*, 80(5):EN127–EN135.

Socco, L. and Boiero, D. (2008). Improved Monte Carlo inversion of surface wave data. *Geophysical Prospecting*, 56(3):357–371.

Socco, L., Boiero, D., Foti, S., and Wisén, R. (2009). Laterally constrained inversion of ground roll from seismic reflection records. *Geophysics*, 74(6):G35–G45.

Socco, L., Foti, S., and Boiero, D. (2010). Surface wave analysis for building near surface velocity models: established approaches and new perspectives. *Geophysics*, 75(5):A83–A102.

Song, X., Tang, L., Lv, X., Fang, H., and Gu, H. (2012). Application of particle swarm optimization to interpret Rayleigh wave dispersion curves. *Journal of Applied Geophysics*, 84:1–13.

Strobbia, C. and Foti, S. (2006). Multi-offset phase analysis of surface wave data (MOPA). *Journal of Applied Geophysics*, 59(4):300–313.

Strobbia, C., Laake, A., Vermeer, P., and Glushchenko, A. (2011). Surface waves: use them then lose them. Surface-wave analysis, inversion and attenuation in land reflection seismic surveying. *Near Surface Geophysics*, 9(6):503–514.

Tarantola, A. (1986). A strategy for nonlinear elastic inversion of seismic reflection data. *Geophysics*, 51(10):1893–1903.

Thomson, W. T. (1950). Transmission of elastic waves through a stratified solid medium. *Journal of applied Physics*, 21(2):89–93.

Tran, K., McVay, M., Faraone, M., and Horhota, D. (2013). Sinkhole detection using 2D full seismic waveform tomography. *Geophysics*, 78(5):R175–R183.

Tran, K. T. and Sperry, J. (2018). Application of 2-D full waveform tomography on land-streamer data for assessment of roadway subsidence. *Geophysics*, 83(3):1–42.

Tsuji, T., Johansen, T. A., Ruud, B. O., Ikeda, T., and Matsuoka, T. (2012). Surface-wave analysis for identifying unfrozen zones in subglacial sediments S-wave velocity in subglacial sediment. *Geophysics*, 77(3):EN17–EN27.

Virieux, J. (1986). P-SV wave propagation in heterogeneous media: velocity-stress finite-difference method. *Geophysics*, 51(4):889–901.

Virieux, J. and Operto, S. (2009). An overview of full-waveform inversion in exploration geophysics. *Geophysics*, 74(6):WCC1–WCC26.

Watson, T. (1970). A note on fast computation of Rayleigh wave dispersion in the multilayered elastic half-space. *Bulletin of the Seismological Society of America*, 60(1):161–166.

Wittkamp, F. and Bohlen, T. (2016). Individual and joint 2-D elastic full waveform inversion of Rayleigh and Love waves. In *78th EAGE Conference and Exhibition 2016*.

Wu, R.-S., Luo, J., and Wu, B. (2014). Seismic envelope inversion and modulation signal model. *Geophysics*, 79(3):WA13–WA24.

Xia, J., Miller, R., and Park, C. (1999). Estimation of near-surface shear-wave velocity by inversion of Rayleigh wave. *Geophysics*, 64(4):691–700.

Xia, J., Xu, Y., Luo, Y., Miller, R., Cakir, C., and Zeng, C. (2012). Advantages of using multichannel analysis of Love waves (MALW) to estimate near-surface shear-wave velocity. *Surveys in Geophysics*, 33(0):841–860.

Xia, J., Xu, Y., Miller, R. D., and Zeng, C. (2010). A trade-off solution between model resolution and covariance in surface-wave inversion. *Pure and Applied Geophysics*, 167(12):1537–1547.

Yamanaka, H. and Ishida, H. (1996). Application of genetic algorithms to an inversion of surface-wave dispersion data. *Bulletin of the Seismological Society of America*, 86(2):436–444.

Yuan, Y. O., Simons, F. J., and Bozdağ, E. (2015). Multiscale adjoint waveform tomography for surface and body waves. *Geophysics*, 80(5):R281–R302.

Zeng, C., Xia, J., Miller, R. D., Tsoflias, G. P., and Wang, Z. (2012). Numerical investigation of MASW applications in presence of surface topography. *Journal of Applied Geophysics*, 84:52–60.

Zhang, S. X. and Chan, L. S. (2003). Possible effects of misidentified mode number on Rayleigh wave inversion. *Journal of Applied Geophysics*, 53(1):17–29.